Coherent dynamics amongst ensembles of spatially and spectrally varying emitters in waveguide QED

L. Ruks,[1,2,*] X. Xu,[1] R. Ohta,[1] W. J. Munro,[2] and V. M. Bastidas[1,2]

[1] *NTT Basic Research Laboratories, NTT Corporation, 3-1 Morinosato Wakamiya, Atsugi, Kanagawa, 243-0198, Japan*
[2] *NTT Research Center for Theoretical Quantum Physics, NTT Corporation, 3-1 Morinosato Wakamiya, Atsugi, Kanagawa, 243-0198, Japan*

(Dated: September 7, 2023)

Spectrally and spatially varying ensembles of emitters embedded into waveguide are ever-present in both well-established and emerging technologies. If control of collective excitations can be attained, a plethora of coherent quantum dynamics and applications may be realized on-chip in the scalable paradigm of waveguide quantum electrodynamics (WQED). Here, we demonstrate how inhomogeneous ensembles embedded into waveguides may be employed as single effective and coherent emitters. The symmetric excitation of localized and mescoscopic ensembles benefit from large collective waveguide coupling, allowing for near-unity and tailorable non-Lorentzian extinction of waveguide photons overcoming large inhomogeneous broadening. As an initial illustration possible in currently existing experiments, we demonstrate the classic recreation of the cavity QED (CQED) paradigm using ensembles of rare-earth ions as coherent mirrors and qubits. This work introduces coherent ensemble dynamics to WQED and extends the realm to spectrally tailorable emitters.

Introduction. Ensembles of emitters in solid state media are a valuable resource for shaping light and processing information as the matter component of hybrid optical platforms [1]. Possible long individual coherence times combined with wide spectral bandwidth [2, 3] of the inhomogeneous line permit applications from quantum memories to atomic frequency combs [4, 5]. When collectively addressed, ensembles enjoy large collective couplings to light and can be employed on the mesoscopic scale as single optical elements [3, 6–9]. Specifically, ensembles embedded into waveguides benefit from well-established telecoms technologies [10–13] whilst allowing for an integrated and scalable optical platform [14, 15]. Despite experimental demonstrations such as potential quantum memories [5, 16, 17] and atomic frequency combs [4, 18], on-chip operation in the framework of waveguide QED [19] remains relatively unexplored theoretically in the naturally occurring and experimentally relevant regime when both spectral inhomogeneity [20, 21] and finite spatial variation [22] are considered. In ordered systems of emitters the waveguide QED paradigm features unique dynamics featuring non-trivial excitation profiles [23] and many-body states [24–26] enabling distinct functionality from CQED, with promise for photonic state generation [27] and quantum simulation [25]. An analogous realisation in inhomogeneous ensembles of solid-state emitters could open the door to a range of applications benefiting from their unique long coherence times and broadband nature, whilst exhibiting naturally scalability when compared with ensemble CQED platforms.

In this work, we establish spatially and spectrally inhomogeneous ensembles of waveguide-embedded emitters as candidates for effective and collectively enhanced optical elements in waveguide QED. We present conditions on spectral and positional inhomogeneity for collective coherence to emerge [28] and establish the symmetric bright-state polariton as a effective and coherent emitter excitation. To treat mescoscopic system sizes of 10^9 emitters, we introduce a method to define collective spins using bins in both space and frequency, enabling a reduction in computational cost and allowing us to demonstrate the formation of emitter coherence via observations of broad and near-unit extinction in the transmission statistics of photons through the waveguide. Interfacing of multiple such emitters then allows for the realisation of the WQED paradigm [19] with spectrally tailorable emitters. As a proof-of-principle we demonstrate the emulation of CQED – including strong coupling – amongst inhomogeneous ensembles of rare-earth ions in analogy with the single-emitter case [24, 29]. We show how the emitter-density threshold required for strong coupling may be considerably reduced within existing experimental capabilities by shaping of the inhomogeneous line using spectral hole burning [30]. Our results suggest that collective excitations in inhomogeneous ensembles can be exploited as effective emitters in near-term technologies within the paradigm of WQED, whilst augmenting this setting with spectral tailorability to explore new regimes of collective ensemble interaction beyond CQED.

The model. In this work we consider N two-level emitters that interact with a continuum of waveguide modes through the standard dipolar light-matter coupling. In addition to rare-earth ions considered here, the following analysis can be applied to systems of hot Doppler-broadened gases [31], quantum dots [32], and NV centers [7]. Assuming weak driving, the emitters in the rotating frame experience a distribution of detunings Δ_j with a full-width-at-half-maximum (FWHM) γ_{inh}. In the regime of weak emitter-field coupling, the field within the waveguide may be traced out to yield the Born-Markov master equation $\dot{\hat{\rho}}_{\text{S}} = -\frac{\mathrm{i}}{\hbar}[\hat{H}, \hat{\rho}_{\text{S}}] + \hat{\mathcal{L}}_{\text{coll}}[\hat{\rho}_{\text{S}}] + \hat{\mathcal{L}}_{\text{ind}}[\hat{\rho}_{\text{S}}]$ for

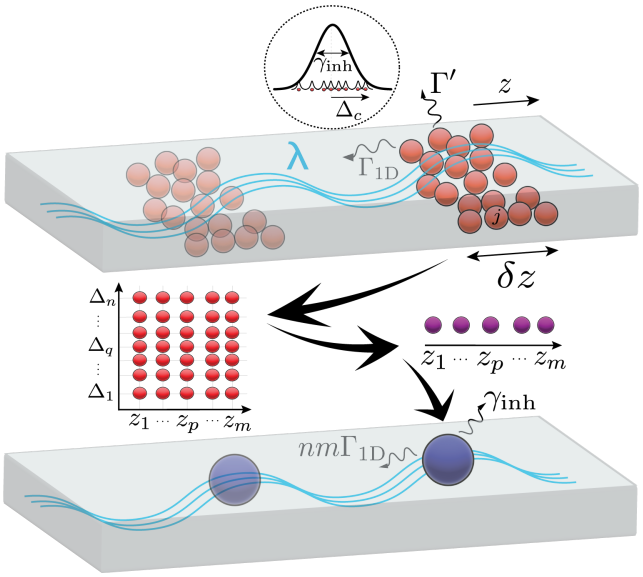

FIG. 1. Binning and formation of a single effective emitter (blue) for a localized ensemble of emitters (red).

emitter density matrix $\hat{\rho}_S$. The Hamiltonian and Lindbladian generating system dynamics are given through the standard spin operators for the j-th emitter, $\hat{\sigma}_j^{\pm}$ and $\hat{\sigma}_j^{ee} = (\hat{\sigma}_j^z + \hat{1})/2$, as follows [19] (with $\{\hat{A}, \hat{B}\} = \hat{A}\hat{B} + \hat{B}\hat{A}$ the anticommutator, while $\Re[w] = \mathrm{Re}[w]$ and $\Im[w] = \mathrm{Im}[w]$ such that $w = \Re[w] + i\Im[w]$, respectively):

$$\begin{aligned}
\hat{H} &= \hat{H}_{\rm em} + \hat{H}_{\rm drv} + \frac{\hbar\Gamma_{1D}}{2}\sum_{j,k=1}^{N} \Im[G_{j,k}]\hat{\sigma}_j^+\hat{\sigma}_k^-, \\
\hat{\mathcal{L}}_{\rm coll}[\hat{\rho}_S] &= \frac{\Gamma_{1D}}{2}\sum_{j,k=1}^{N} \Re[G_{j,k}]\left(2\hat{\sigma}_k^-\hat{\rho}_S\hat{\sigma}_j^+ - \{\hat{\sigma}_j^+\hat{\sigma}_k^-, \hat{\rho}_S\}\right) \\
\hat{\mathcal{L}}_{\rm ind}[\hat{\rho}_S] &= \frac{\Gamma'}{2}\sum_{j=1}^{N}\left(2\hat{\sigma}_j^-\hat{\rho}_S\hat{\sigma}_j^+ - \{\hat{\sigma}_j^+\hat{\sigma}_j^-, \hat{\rho}_S\}\right) \qquad (1)
\end{aligned}$$

Here the single-body effects are present in the frequency distribution, $\hat{H}_{\rm em} = \hbar\sum_{j=1}^{N}\Delta_j\hat{\sigma}_j^{ee}$, a weak coherent driving $\hat{H}_{\rm drv} = \hbar\sum_j \Omega_j(\hat{\sigma}_j^+ + \sigma_j^-)$ and individual emitter decay with rate Γ' [33]. Crucially, the waveguide-mediated emitter-emitter interactions are subject to infinite-range interactions through the 1D propagator $G_{j,k} = e^{i\beta|z_{j,k}|}$, where $z_{j,k} = z_j - z_k$ with z_j being the position of the j-th emitter. Γ_{1D} is the single-emitter decay rate into the waveguide, and $\beta = 2\pi/\lambda$ is the wavenumber of the (assumed single) waveguided mode with wavelength λ. To address mesoscopic sizes of $N = 10^9$ and beyond in the general presence of inhomogeneity, we approximate the spatial-spectral density in the large-number limit as a decorrelated product of position and frequency densities such that each individual emitter lies in some designated frequency bin and position bin (Fig. 1). The symmetric states may then form levels of effective emitters (see Supplemental Material (SM) [34] for details), under conditions and a procedure that follows.

Treating inhomogeneous broadening for single ensembles. Assuming that there are n frequency bins and m positional bins with $nm = N$, we relabel each spin j with two indices $j \to (p, q)$ such that $\hat{\sigma}_{p,q}^{ee}$ and $\hat{\sigma}_{p,q}^{\pm}$ correspond to the emitter in the p-th positional bin and the q-th frequency bin. Noting from Eq. (1) that only frequencies can distinguish spins in a given position bin, we consider the regime of weak spin saturation where product averages decorrelate $\langle\hat{\sigma}_j^{\alpha}\hat{\sigma}_l^{\beta}\rangle \approx \langle\hat{\sigma}_j^{\alpha}\rangle\langle\hat{\sigma}_l^{\beta}\rangle$ for $j \neq l$ and where excited state population is negligible $\langle\sigma_j^{ee}\rangle \approx 0$ for all j. This allows us to obtain the equations of motion for averages $\bullet := \langle\hat{\bullet}\rangle$:

$$\dot{\sigma}_{p,q}^- = i\Delta_{p,q}\sigma_{p,q}^- - \frac{\Gamma'}{2}\sigma_{p,q}^- - \mathcal{A}_p^-, \qquad (2)$$

where $\mathcal{A}_p^-$ is a q-independent linear function of all lowering operators containing the interactions from Eq. (1). For each positional bin p we define a symmetric operator [35] (purple emitter, Fig. 1),

$$\hat{\mathcal{B}}_p^- = \frac{1}{\sqrt{n}}\sum_{q=1}^{n}\hat{\sigma}_{p,q}^-, \qquad (3)$$

and assuming that frequency distributions $\Delta_{p,q}$ are identical for each p, we find in the steady-state that population is determined via the linear-response relation:

$$\mathcal{B}_p^- = i\sqrt{n}\gamma_{\rm inh}^{-1}\chi(\Delta_c)\mathcal{A}_p^-, \qquad (4)$$

For this derivation, we have taken the continuum limit such that $\frac{1}{n}\sum_l \to \int d\Delta'\rho(\Delta')$ for identical spectral densities $\rho_p(\Delta_c) = \rho(\Delta_c)$ (defined with respect to detuning Δ_c from the average of the inhomogeneous line), and where the ensemble response function is defined $\chi(\Delta_c) = \gamma_{\rm inh}\int \frac{d\Delta'\rho(\Delta')}{\Delta' - \Delta_c - i\frac{\Gamma'}{2}}$. Steady-state dynamics correspond to that generated by the effective non-Hermitian Hamiltonian between bright states:

$$\begin{aligned}
\hat{H}_{\rm eff}^{\rm nh} = &-in\tfrac{\Gamma_{1D}}{2}\textstyle\sum_{p,p'=1}^{m} G_{p,p'}\hat{\mathcal{B}}_p^+\hat{\mathcal{B}}_{p'}^- \\
&+\textstyle\sum_{p=1}^{m}(\gamma_{\rm inh}\chi^{-1}(\Delta_c) - i\tfrac{\Gamma'}{2})\hat{\mathcal{B}}_p^+\hat{\mathcal{B}}_p^-. \qquad (5)
\end{aligned}$$

Note that the collective bright-state interactions see an enhancement by n [28, 36] over the single-body terms, including broadening. For our system of interest, bright-state and broadening-induced resonance dominate narrow single-emitter resonances, $\Gamma' \ll \gamma_{\rm inh}, N\Gamma_{1D}$, so in the following analysis we implicitly take $\Gamma' \to 0^+$.

Transmission statistics. Extending beyond the case of Lorentzian emitters [37], we obtain the transmission coefficient through the waveguide:

$$t(\Delta_c) = \prod_{\mu=1}^{m}\left(\frac{\gamma_{\rm inh}\chi^{-1}(\Delta_c) + i\Gamma'/2}{\gamma_{\rm inh}\chi^{-1}(\Delta_c) + i\Gamma'/2 + \Lambda_\mu}\right), \qquad (6)$$

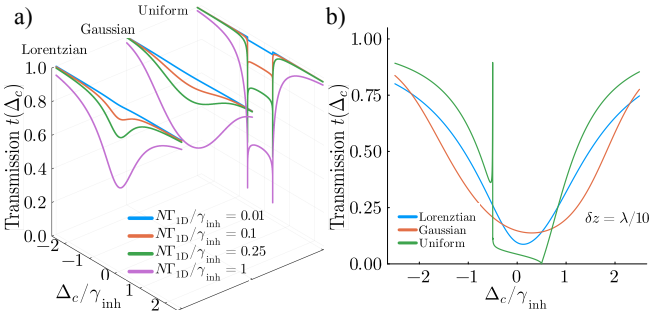

FIG. 2. Single-ensemble transmission. (a) Transmission through ensembles featuring no positional inhomogeneity as the collective waveguide coupling efficiency $N\Gamma_{1D}/\gamma_{inh}$ is increased for each of the three prototypical spectral distributions. The effect of Γ' is neglected. (b) Transmission profile for ensembles of $N = 10^9$ emitters with $\gamma_{inh}/(2\pi) = 50$GHz, $\Gamma_{1D}/(2\pi) = \Gamma'/(2\pi) = 100$Hz. We consider $n = 10^6$ frequency bins and $m = 10^3$ positional bins, and show for one realization of random positions on $[0, \delta z]$.

where $\Lambda_\mu = \omega_\mu + i\Gamma_\mu/2$ are the complex energy eigenvalues of $[\frac{in\Gamma_{1D}}{2}G_{p,p'}]_{pp'}$, i.e., the collective symmetric-state interaction of Eq. (5). Generally, a large $|\Delta_c| \gg \gamma_{inh}$ expansion yields the shift $\Delta_c - \gamma_{inh}\chi^{-1}(\Delta_c) \sim -i\pi\Delta_c^2\rho(\Delta_c) + O(\gamma_{inh}^2/\Delta_c)$ at leading order in Γ'. A well-known consequence [6, 35] is that the effective decay rate experienced by finite-variance (i.e., sub-Lorentzian) inhomogeneous lines such that $\Delta_c^2\rho(\Delta_c) \to 0$ for $|\Delta_c| \to \infty$ are $\Gamma'/2$-limited for large detuning, and in our case more precisely $(\Gamma'+\Gamma_\mu)/2$-limited once $|\Delta_c| \gtrapprox \gamma_{inh}$. In applications, a desired response and effective decay-rate may be reverse-engineered via the relation $\rho(\Delta_c) = \frac{1}{\pi\Delta}\Im[\chi(\Delta_c)]$.

Coherent extinction. Similarly to the case of single emitters [29, 38], an inhomogeneous ensemble of emitters may act as a coherent mirror [39, 40] for waveguided photons when the collective decay process exceeds the (effective) single-emitter linewidth. Here, the effective single-emitter linewidth is approximately set by the inhomogeneous linewidth. As can be seen from Eq. (6), then for identical positions with $m = 1$ the condition

$$\Gamma_\mu/\gamma_{inh} = N\Gamma_{1D}/\gamma_{inh} \gg 1, \tag{7}$$

yields an appreciable and broad extinction resonance in the transmission, as can be seen in Fig. 2(b) for the prototypical spectral distributions of FWHM γ_{inh} defined in the SM. This also coincides with the condition for the right-hand side in Eq. 4 to become appreciable, and establish significant polarization $\mathcal{B}_p^-$. When Eq. (7), the collective process dominates and the extinction coefficient is approximately equal to that of reflection [29]. In addition, establishing of the resonance is accompanied by an appreciable phase shift of the transmitted photon [41]. The onset of high quality reflectance can be seen to be advanced over frequency regions by shaping the spectral distribution using spectral hole burning. This effect can greatly relax density requirements for observing coherence, and holds up in the presence of positional fluctuations, treated in the following.

Inclusion of positional inhomogeneity. Positional disorder on the scale $\delta z \lessapprox 0.1\lambda$ can be achieved in a variety of optical platforms [42–44], and via ion-implantation specifically in the case of rare-earth ions [43]. In addition, well-below subwavelength confinement is available to microwave-based platforms [7] and so we here restrict our analysis to the perturbative regime $\delta z \ll \lambda$. When small positional inhomogeneity δz along the waveguide is present, formerly inaccessible resonances attain a finite linewidth [19, 45], which results in a cascade of narrow lines within the center of the broad resonances observed in Fig. 2. In order to maintain coherent mirror-like operation, the broad resonance of the bright state should be maintained such that any perturbation is limited to relatively narrow transparency windows. The broadest resonances feature slowly varying polarizations over the length of the ensemble, and so remain relatively unperturbed with respect for positional fluctuations for large N. Assuming a uniform density on $[0, \delta z]$, the approximate *bin-independent* eigenvalues of the brightest states are derived in Appendix to order $O(\nu^2)$ for $\nu = \beta\delta z \ll 1$:

$$\Lambda_0 = \tfrac{N\Gamma_{1D}}{2}\left(-\tfrac{\nu}{3} + i\left[1 - \tfrac{4\nu^2}{45}\right]\right), \tag{8}$$

$$\Lambda_\mu = \tfrac{N\Gamma_{1D}}{2}\left(\tfrac{2\nu}{\mu^2\pi^2} + i\tfrac{8\nu^2}{\mu^4\pi^4}\right) \quad (1 \le \mu \ll m), \tag{9}$$

and we see that the effect of increasing m (equivalently N) is to introduce increasingly narrow resonances [45] that do not concern us here. The *N-independent* condition on linewidths, $\Im[\Lambda_1] \lessapprox \Im[\Lambda_0]$, for coherent single-mode operation is then obtained,

$$\delta z \lessapprox 2\lambda/5, \tag{10}$$

which is well satisfied by $\delta z = 0.1\lambda$ already preserving the broad resonance, as seen in Fig. 2(b). Finally, for a single spatially localized ensemble one may form the bright state (blue emitter, Fig. 1) operator $\hat{\mathfrak{B}}^- = \frac{1}{\sqrt{m}}\sum_{p=1}^m \hat{\mathcal{B}}_p^-$. When multiple ensembles are present, expectations of such bright state operators alone well approximate dynamics on sufficiently short time scales. As detailed in Appendix , a total approximate rate of loss of the bright state to the narrow resonances is given by $\frac{N\Gamma_{1D}}{2}\left(\frac{\delta z}{\lambda}\right)$, which is at least an order of magnitude smaller than the bright-state processes for our considered δz. In contrast to inhomogeneous broadening, the collective resonances due to positional inhomogeneity are enhanced with increasing N, and so the demand (10) must be respected. When this is the case, coherent processes may occur between ensembles, as demonstrated in the following.

Emulation of CQED. The combined use of localized emitter ensembles satisfying the collective threshold condition (7) and the single-moded condition (10) can emulate two mirrors and a qubit placed along the waveguide, forming an *in situ* optical cavity [24]. Assuming

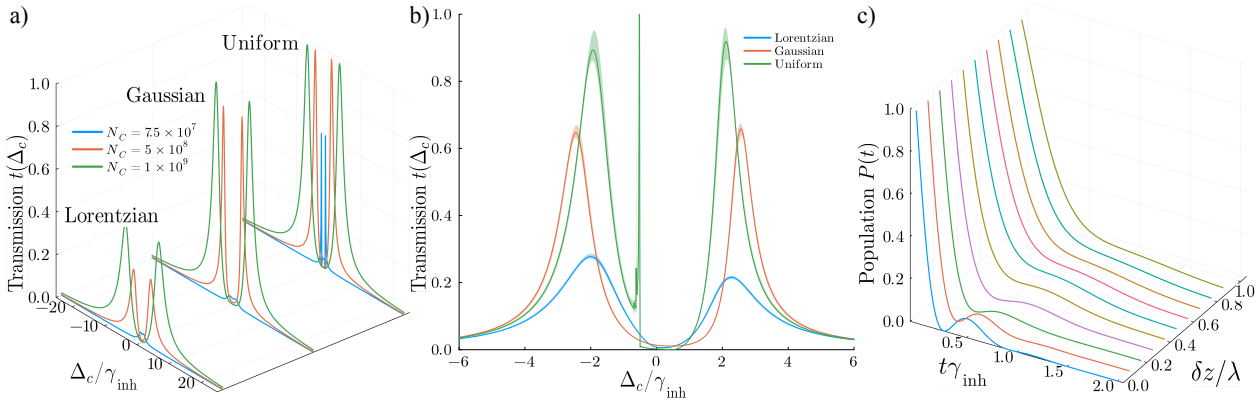

FIG. 3. Strong coupling in the effective atom-cavity system. (a) Development of the peak splitting for side-illumination with increasing emitter number N_C in the cavity ensembles. We take waveguide decay rates as in Fig. 2, and broadening $\gamma_{\rm inh}/(2\pi) = 10$GHz, with $\Gamma_{1D}/(2\pi) = \Gamma'/(2\pi) = 100$Hz. (b) Transmission spectrum for a single realization of random positions for fluctuations $\delta z = 0.1\lambda, \gamma_{\rm inh}/(2\pi) = 10$GHz, $2N_Q = N_C = 4 \times 10^8$. The shaded regions give the bounds of transmission obtained over 100 realizations of random positions. The qubit ensemble is additionally detuned (in practice can be achieved by, e.g., surface acoustic waves [3]) to counter the mirror-qubit detuning that arises according to according to Eq. 8, which results in an effective cavity-qubit detuning and ordinarily asymmetric peaks. (c) Loss of Rabi oscillations of the qubit population $P(t)$ with increasing positional fluctuations for Lorenztian spectral broadening. A single realization of positions is chosen in each case. Parameters are identical to (b), but we here choose $2N_Q = N_C = 1 \times 10^9$.

N_Q emitters in a designated qubit ensemble with bright state polarization $\mathcal{B}_Q^-$, and N_C emitters each in two designated cavity mirror ensembles, then when the mirror ensembles are spaced $\lambda/2 + r\lambda$ (integer r) with the qubit ensemble at their midpoint, the qubit interaction with the photonic component of the eigenstates formed by the mirrors is Hamiltonian. For illustration, assuming Lorentzian broadening and forming the cavity dark state polarization $\hat{\mathcal{B}}_C^-$ as the bright state of the mirror bright states, the equations of motion describing CQED are obtained as initially proposed in [29]:

$$\dot{\mathcal{B}}_Q^- = [\mathrm{i}\Delta_c - (\tfrac{N_Q\Gamma_{1D}+\gamma_{\rm inh}}{2})]\mathcal{B}_Q^- + \mathrm{i}\sqrt{2N_QN_C}\tfrac{\Gamma_{1D}}{2}\mathcal{B}_C^- \quad (11)$$

$$\dot{\mathcal{B}}_C^- = (\mathrm{i}\Delta_c - \tfrac{\gamma_{\rm inh}}{2})\mathcal{B}_C^- + \mathrm{i}\sqrt{2N_QN_C}\tfrac{\Gamma_{1D}}{2}\mathcal{B}_Q^-. \quad (12)$$

The analogy to CQED is made with qubit decay rate γ, cavity decay rate κ, and coupling g respectively:

$$\gamma = N_Q\Gamma_{1D} + \gamma_{\rm inh} \qquad \kappa = \gamma_{\rm inh}, \qquad g = \sqrt{\frac{N_QN_C}{2}}\Gamma_{1D}.$$

Notably, for $N_q \sim N_c \sim N$ we have additionally have $g \sim N\Gamma_{1D}$, a square root enhancement in N over conventional cavities [35]. In the strong-coupling regime, the two eigenvalues

$$\Lambda^{\pm} = \pm\frac{\Gamma_{1D}}{2}\sqrt{8N_QN_C - N_Q^2} - \mathrm{i}\left(\frac{N_Q\Gamma_{1D}}{4} + \frac{\gamma_{\rm inh}}{2}\right) \quad (13)$$

are present. For finite-variance mirror-symmetric inhomogeneous lines one may approximate decay rates about the peaks as $\gamma_{\rm inh} \to \pi\Re[\Lambda^{\pm}]^2\rho\left(\Re[\Lambda^{\pm}]\right)$, which limits γ and κ to $N_Q\Gamma_{1D}$ (*into the waveguide*) and 0 respectively. Whilst the generic conditions to be well within the strong coupling regime approximately read $\sqrt{N_CN_Q} \gg \frac{\gamma_{\rm inh}}{\Gamma_{1D}}, 2N_C \geq N_Q$, there is then significant variation in the onset of peak visibility for differing spectral distributions. Applying a side illumination scheme to avoid exciting the broad mirror resonance [24], this effect can be observed in Fig. 3(a), first considering the case of $\delta z = 0$. For conservative parameters $\gamma_{\rm inh}/(2\pi) = 10$GHz, and $\Gamma_{1D}/(2\pi) = \Gamma'/(2\pi) = 100$Hz corresponding to the optical Erbium transition $Y_1 \to Z_1$ implanted into YSO [3] or grown in rare-earth oxides [4, 46], peaks are established in the Gaussian and uniform case for individual ensemble numbers as low as $N = 10^8$, which for emitters localized in a region of size $\delta z \times \lambda^2 = 0.1\lambda \times \lambda^2 = 0.1\lambda^3$ corresponds to doping concentrations below the achievable $10^{22}\mathrm{cm}^{-3}$ [46]. Reintroducing positional inhomogeneity, we see in Fig. 3(b) that for the experimentally accessible regime of $\delta z \approx 0.1\lambda$, high visibility peaks are still retained, with the effect of finite spatial extent limited to narrow central resonances. The corresponding Rabi oscillations of the bright state population in Fig. 3(c) are preserved for regimes of smaller spatial extent even in the lowest-fidelity Lorentzian case and illustrate coherent population transfer between the two modes. Note that by using, e.g., photonic crystal waveguides [47, 48] or plasmonics [49] to enhance Γ_{1D}, the density requirements for constant peak visibility can be reduced by 1-2 orders of magnitude, or peak visibility enhanced for constant N. With optical wavelengths on the order of μm and possible waveguide lengths on the order of mm, the local density within a single ensemble can be reduced even further orders of magnitude by employing commensurate ensembles along the waveguide as a single unit [29]. For

microwave transitions the long wavelength allows orders of magnitude more emitters in a given wavelength, and also offers a promising platform for observing strong coupling.

Conclusion. In this work we demonstrated that the bright states of ensembles of spatially localized and inhomogeneously broadened rare-earth ions can be employed as coherent and spectrally tailorable emitters in the paradigm of waveguide QED and in currently accessible and near-term experimental platforms. When sufficiently localized in space and when the linewidth of a collective resonance exceeds that of inhomogeneous broadening, the single resonance becomes accessible in the spectrum, allowing for the formation of coherent optical elements. As such, the strong coupling regime of CQED can be readily accessed with low emitter concentrations when spectral hole burning is additionally employed. These results suggest the potential of the inhomogeneous ensembles for coherent dynamics in optical waveguides beyond extended bulk applications, and advance the theory of mesoscopic systems of optical emitters.

Acknowledgments.— The authors acknowledge valuable discussions with K. Azuma

* Lewis.ruks@ntt.com

[1] G. Kurizki, P. Bertet, Y. Kubo, K. Mølmer, D. Petrosyan, P. Rabl, and J. Schmiedmayer, Quantum technologies with hybrid systems, Proc. Nat. Acad. Sci. USA **112**, 3866 (2015).

[2] D. Serrano, S. K. Kuppusamy, B. Heinrich, O. Fuhr, D. Hunger, M. Ruben, and P. Goldner, Ultra-narrow optical linewidths in rare-earth molecular crystals, Nature **603**, 241 (2022).

[3] R. Ohta, L. Herpin, V. M. Bastidas, T. Tawara, H. Yamaguchi, and H. Okamoto, Rare-earth-mediated optomechanical system in the reversed dissipation regime, Phys. Rev. Lett. **126** (2021).

[4] S. Yasui, M. Hiraishi, A. Ishizawa, H. Omi, T. Inaba, X. Xu, R. Kaji, S. Adachi, and T. Tawara, Creation of a high-resolution atomic frequency comb and optimization of the pulse sequence for high-efficiency quantum memory in ^{167} Er:Y_2SiO_5, Opt. Cont. **1**, 1896 (2022).

[5] D. Lago-Rivera, S. Grandi, J. V. Rakonjac, A. Seri, and H. de Riedmatten, Telecom-heralded entanglement between multimode solid-state quantum memories, Nature **594**, 37 (2021).

[6] T. Zhong, J. M. Kindem, J. Rochman, and A. Faraon, Interfacing broadband photonic qubits to on-chip cavity-protected rare-earth ensembles, Nat. Comm. **8** (2017).

[7] X. Zhu, S. Saito, A. Kemp, K. Kakuyanagi, S. ichi Karimoto, H. Nakano, W. J. Munro, Y. Tokura, M. S. Everitt, K. Nemoto, M. Kasu, N. Mizuochi, and K. Semba, Coherent coupling of a superconducting flux qubit to an electron spin ensemble in diamond, Nature **478**, 221 (2011).

[8] R. Amsüss, C. Koller, T. Nöbauer, S. Putz, S. Rotter, K. Sandner, S. Schneider, M. Schramböck, G. Steinhauser, H. Ritsch, J. Schmiedmayer, and J. Majer, Cavity QED with magnetically coupled collective spin states, Phys. Rev. Lett. **107** (2011).

[9] M. Lei, R. Fukumori, J. Rochman, B. Zhu, M. Endres, J. Choi, and A. Faraon, Many-body cavity quantum electrodynamics with driven inhomogeneous emitters, Nature **617**, 271 (2023).

[10] P. M. Becker, A. A. Olsson, and J. R. Simpson, *Erbium-doped fiber amplifiers: fundamentals and technology* (Elsevier, 1999).

[11] S. Rinner, F. Burger, A. Gritsch, J. Schmitt, and A. Reiserer, Erbium emitters in commercially fabricated nanophotonic silicon waveguides, Nanophotonics (2023).

[12] L. Weiss, A. Gritsch, B. Merkel, and A. Reiserer, Erbium dopants in nanophotonic silicon waveguides, Optica **8**, 40 (2021).

[13] O. E. Mor, T. Ohana, A. Borne, Y. Diskin-Posner, M. Asher, O. Yaffe, A. Shanzer, and B. Dayan, Tapered optical fibers coated with rare-earth complexes for quantum applications, ACS Phot. **9**, 2676 (2022).

[14] A. Sipahigil, R. E. Evans, D. D. Sukachev, M. J. Burek, J. Borregaard, M. K. Bhaskar, C. T. Nguyen, J. L. Pacheco, H. A. Atikian, C. Meuwly, R. M. Camacho, F. Jelezko, E. Bielejec, H. Park, M. Lončar, and M. D. Lukin, An integrated diamond nanophotonics platform for quantum-optical networks, Science **354**, 847 (2016).

[15] A. Faraon, A. Majumdar, D. Englund, E. Kim, M. Bajcsy, and J. Vučković, Integrated quantum optical networks based on quantum dots and photonic crystals, New J. Phys. **13**, 055025 (2011).

[16] K. S. Choi, H. Deng, J. Laurat, and H. J. Kimble, Mapping photonic entanglement into and out of a quantum memory, Nature **452**, 67 (2008).

[17] B. Julsgaard, C. Grezes, P. Bertet, and K. Mølmer, Quantum memory for microwave photons in an inhomogeneously broadened spin ensemble, Phys. Rev. Lett. **110** (2013).

[18] M. Afzelius, C. Simon, H. de Riedmatten, and N. Gisin, Multimode quantum memory based on atomic frequency combs, Phys. Rev. A **79** (2009).

[19] A. S. Sheremet, M. I. Petrov, I. V. Iorsh, A. V. Poshakinskiy, and A. N. Poddubny, Waveguide quantum electrodynamics: collective radiance and photon-photon correlations, Rev. of Mod. Phys. **95**, 015002 (2023).

[20] T. Kling and M. Hosseini, Characteristics of 1D ordered arrays of optical centers in solid-state photonics, J. Phys: Phot. **5**, 024003 (2023).

[21] G.-Z. Song, J.-L. Guo, W. Nie, L.-C. Kwek, and G.-L. Long, Optical properties of a waveguide-mediated chain of randomly positioned atoms, Opt. Express **29**, 1903 (2021).

[22] J. Ruostekoski and J. Javanainen, Emergence of correlated optics in one-dimensional waveguides for classical and quantum atomic gases, Phys. Rev. Lett. **117**, 143602 (2016).

[23] E. Kim, X. Zhang, V. S. Ferreira, J. Banker, J. K. Iverson, A. Sipahigil, M. Bello, A. González-Tudela, M. Mirhosseini, and O. Painter, Quantum electrodynamics in a topological waveguide, Phys. Rev. X **11**, 011015 (2021).

[24] M. Mirhosseini, E. Kim, X. Zhang, A. Sipahigil, P. B. Dieterle, A. J. Keller, A. Asenjo-Garcia, D. E. Chang, and O. Painter, Cavity quantum electrodynamics with atom-like mirrors, Nature **569**, 692 (2019).

[25] J. S. Douglas, H. Habibian, C.-L. Hung, A. V. Gorshkov, H. J. Kimble, and D. E. Chang, Quantum many-body models with cold atoms coupled to photonic crystals, Nat. Phot. **9**, 326 (2015).

[26] T. F. See, V. M. Bastidas, J. Tangpanitanon, and D. G. Angelakis, Strongly correlated photon transport in nonlinear photonic lattices with disorder: Probing signatures of the localization transition, Phys. Rev. A **99**, 033835 (2019).

[27] A. González-Tudela, V. Paulisch, H. Kimble, and J. I. Cirac, Efficient multiphoton generation in waveguide quantum electrodynamics, Phys. Rev. Lett. **118**, 213601 (2017).

[28] C. Braggio, F. Chiossi, G. Carugno, A. Ortolan, and G. Ruoso, Spontaneous formation of a macroscopically extended coherent state, Phys. Rev. Res. **2** (2020).

[29] D. E. Chang, L. Jiang, A. V. Gorshkov, and H. J. Kimble, Cavity QED with atomic mirrors, New J. Phys. **14**, 063003 (2012).

[30] W. E. Moerner and G. C. Bjorklund, *Persistent spectral hole-burning: science and applications*, Vol. 1 (Springer, 1988).

[31] R. Ritter, N. Gruhler, H. Dobbertin, H. Kübler, S. Scheel, W. Pernice, T. Pfau, and R. Löw, Coupling thermal atomic vapor to slot waveguides, Phys. Rev. X **8**, 021032 (2018).

[32] J. C. Norman, D. Jung, Z. Zhang, Y. Wan, S. Liu, C. Shang, R. W. Herrick, W. W. Chow, A. C. Gossard, and J. E. Bowers, A review of high-performance quantum dot lasers on silicon, IEEE J. Quantum Electron. **55**, 1 (2019).

[33] Γ' may include photonic decay into unguided modes, or non-radiative decay into, e.g., material phonons.

[34] See Supplemental Material at link for additional details on the binning procedure, the calculation of the response functions, the eigenvalue approximation and the perturbative coupling to dark states.

[35] I. Diniz, S. Portolan, R. Ferreira, J. Gérard, P. Bertet, and A. Auffeves, Strongly coupling a cavity to inhomogeneous ensembles of emitters: Potential for long-lived solid-state quantum memories, Phys. Rev. A **84**, 063810 (2011).

[36] F. L. Kien and K. Hakuta, Cooperative enhancement of channeling of emission from atoms into a nanofiber, Phys. Rev. A **77** (2008).

[37] A. Asenjo-Garcia, J. Hood, D. Chang, and H. Kimble, Atom-light interactions in quasi-one-dimensional nanostructures: A Green's-function perspective, Phys. Rev. A **95**, 033818 (2017).

[38] Z. Liao, X. Zeng, H. Nha, and M. S. Zubairy, Photon transport in a one-dimensional nanophotonic waveguide qed system, Phys. Scripta **91**, 063004 (2016).

[39] X. Li and L. F. Wei, Designable single-photon quantum routings with atomic mirrors, Phys. Rev. A **92** (2015).

[40] A. Nandi, H. An, and M. Hosseini, Coherent atomic mirror formed by randomly distributed ions inside a crystal, Opt. Lett. **46**, 1880 (2021).

[41] P. Domokos, P. Horak, and H. Ritsch, Quantum description of light-pulse scattering on a single atom in waveguides, Physical Review A **65** (2002).

[42] Y. Meng, A. Dareau, P. Schneeweiss, and A. Rauschenbeutel, Near-ground-state cooling of atoms optically trapped 300 nm away from a hot surface, Phys. Rev. X **8**, 031054 (2018).

[43] D. Pak, A. Nandi, M. Titze, E. S. Bielejec, H. Alaeian, and M. Hosseini, Long-range cooperative resonances in rare-earth ion arrays inside photonic resonators, Comm. Phys. **5**, 89 (2022).

[44] M. Pfeiffer, K. Lindfors, H. Zhang, B. Fenk, F. Phillipp, P. Atkinson, A. Rastelli, O. G. Schmidt, H. Giessen, and M. Lippitz, Eleven nanometer alignment precision of a plasmonic nanoantenna with a self-assembled gaas quantum dot, Nano Lett. **14**, 197 (2014).

[45] Y.-X. Zhang and K. Mølmer, Theory of subradiant states of a one-dimensional two-level atom chain, Phys. Rev. Lett. **122**, 203605 (2019).

[46] X. Xu, T. Inaba, T. Tsuchizawa, A. Ishizawa, H. Sanada, T. Tawara, H. Omi, K. Oguri, and H. Gotoh, Low-loss Erbium-incorporated rare-earth oxide waveguides on Si with bound states in the continuum and the large optical signal enhancement in them, Opt. Exp. **29**, 41132 (2021).

[47] E. Viasnoff-Schwoob, C. Weisbuch, H. Benisty, S. Olivier, S. Varoutsis, I. Robert-Philip, R. Houdré, and C. Smith, Spontaneous emission enhancement of quantum dots in a photonic crystal wire, Phys. Rev. Lett. **95**, 183901 (2005).

[48] V. M. Rao and S. Hughes, Single quantum-dot Purcell factor and β factor in a photonic crystal waveguide, Phys. Rev. B **75**, 205437 (2007).

[49] N. A. Güsken, M. Fu, M. Zapf, M. P. Nielsen, P. Dichtl, R. Röder, A. S. Clark, S. A. Maier, C. Ronning, and R. F. Oulton, Emission enhancement of erbium in a reverse nanofocusing waveguide, Nature Communications **14** (2023).

[50] M. R. Vladimirova, E. L. Ivchenko, and A. V. Kavokin, Exciton polaritons in long-period quantum-well structures, Semiconductors **32**, 90 (1998).

Considerations for the binning procedure

Given the $n \times m$ binning procedure of N emitters, both n and m must be chosen large enough to allow for their respective continuum approximations to be valid so that bright-state dynamics may be well approximated. In addition, after the renormalization over frequency is made, the resulting system matrix for steady-state dynamics is $m \times m$, which should be small enough to allow numerical computation of eigenvalues (i.e., $m \sim 10^4$ for a standard desktop. For positional fluctuations much smaller than a wavelength, $n = 10^6$ and $m = 10^3$ produce satisfactory results in the main text with small fluctations over individual realisations [as in Fig. 3(b)] and small variation as n, m are varied with constant $nm = N$. The results are expected to remain satisfactory for smaller N such that $n \gtrapprox 10^3$. For smaller system sizes than this exact numerical computation should be then feasible.

Response functions

We here list the well-known results [35] of (unnormalized) response functions $W_s(\Delta_c) = \int \frac{d\Delta' \rho_s(\Delta')}{\Delta' - \Delta_c - i\Gamma'/2}$ for Gaussian ($s = g$), Uniform ($s = u$), and Lorentzian

$(s = l)$ distributions with a FWHM $\gamma_{\rm inh}$ respectively as follows:

$$W_g(\Delta_c) = -\frac{\sqrt{\pi}}{\mathrm{i}\gamma_{\rm inh}/2}\frac{\sqrt{\ln 2}}{2}\mathrm{erfcx}\left(\frac{\sqrt{\ln 2}}{2}\frac{\Delta_c + \mathrm{i}\Gamma'/2}{\mathrm{i}\gamma_{\rm inh}/2}\right) \tag{14}$$

$$W_u(\Delta_c) = -\frac{1}{\mathrm{i}\gamma_{\rm inh}/2}\arctan\left(\frac{\mathrm{i}\gamma_{\rm inh}/2}{\Delta_c + \mathrm{i}\Gamma'/2}\right) \tag{15}$$

$$W_l(\Delta_c) = -\frac{1}{\Delta_c + \mathrm{i}(\Gamma' + \gamma_{\rm inh})/2}, \tag{16}$$

where the densities read

$$\rho_g(\Delta_c) = \frac{1}{(\gamma_{\rm inh}/\sqrt{\ln 2})\sqrt{\pi}}e^{-\Delta_c^2/(\gamma_{\rm inh}/\sqrt{\ln 2})^2} \tag{17}$$

$$\rho_u(\Delta_c) = \frac{\chi_{[-\gamma_{\rm inh}/2,\gamma_{\rm inh}/2]}}{\gamma_{\rm inh}} \tag{18}$$

$$\rho_l(\Delta_c) = \frac{(\gamma_{\rm inh}/2)}{\pi}\frac{1}{(\gamma_{\rm inh}/2)^2 + \Delta_c^2}, \tag{19}$$

with the indicator function $\chi_{[a,b]}$ taking value 1 in $[a, b]$ and 0 otherwise.

Eigenvalue approximation

To obtain analytical expressions we consider the distributions of atoms uniform on $[0, \delta z]$ and with equal spacing $\delta z/M$. At the expense of neglecting to treat states with smaller decay rates, the eigenvalues of the pseudo-random, equally spaced system can well reproduce behaviour on the shorter time scales associated with the brighter states even in the fully random system. This is due to the fact that the brightest states are associated with long-wavelength spin waves, which are negligibly perturbed by the positional fluctuations on much shorter length scales. Assuming emitter density is high (i.e., many emitters in a given wavelength), we move to the continuum limit:

$$\frac{\mathrm{i}N\Gamma_{\rm 1D}}{2}\int_0^{\delta z}\frac{dz'}{\delta z}\exp(\mathrm{i}\beta|z - z'|)\sigma_k(z') = \lambda_k\sigma_k(z), \tag{20}$$

which can be transformed to the unit interval:

$$\frac{\mathrm{i}N\Gamma_{\rm 1D}}{2}\int_0^{1} dZ'\exp(\mathrm{i}\nu|Z - Z'|)\tilde{\sigma}_k(Z') = \lambda_k\tilde{\sigma}_k(Z), \tag{21}$$

where $Z = z/(\delta z)$ and $\sigma(z)$ is the spin profile at continuum position z, and $\tilde{\sigma}_l(Z) = \sigma_k(z)$. Whilst the uniform distribution is considered here, the corresponding expression for general distribution immediately shows that in the high density limit the existing eigenvalues of the system are unchanging up to a scaling with m, regardless of the underlying positional distribution. Similarly to the discrete case [50], the spin profile

$$\tilde{\sigma}_\mu(Z) = \mathcal{N}_\mu\left(e^{\mathrm{i}k_\mu Z} + e^{\mathrm{i}\phi_\mu}e^{-\mathrm{i}k_\mu Z}\right), \tag{22}$$

yields the eigenvalue

$$\Lambda_\mu = \frac{\mathrm{i}N\Gamma_{\rm 1D}}{2}\frac{2\mathrm{i}\nu}{\nu^2 - k_\mu^2} \tag{23}$$

subject to the consistency condition

$$\left(\frac{k_\mu + \nu}{k_\mu - \nu}\right)^2 = e^{2\mathrm{i}k_\mu} = e^{2\mathrm{i}\phi_\mu}, \tag{24}$$

for normalization factor $\mathcal{N}_\mu$, which holds for arbitrary ensemble extent in the high density limit. The limit $\nu = 0$ yields $k_\mu = \mu\pi, \mu = 0, 1, \ldots$, corresponding to $m-1$ states with zero decay rate and the single bright state (for which a more careful limiting argument is required). Assuming $\nu \ll \pi$, one may perturbatively solve (24) for $\mu \geq 1$ to yield the approximate spin wavenumbers

$$k_\mu = \mu\pi - \frac{2\mathrm{i}}{\mu\pi}\nu + \frac{4}{\mu^3\pi^3}\nu^2 + O(\nu^3), \tag{25}$$

whilst for $\mu = 0$, k_μ scales as $\sqrt{\nu}$. One can carry out the perturbation analysis or just note the trace property $\sum_{\mu=0}^{\infty}\Lambda_\mu = \frac{\mathrm{i}N\Gamma_{\rm 1D}}{2}$. Inserting k_μ into the eigenvalue and using this relation (and standard identities for $\sum_{s=1}^{\infty}\frac{1}{s^2}$, etc.,) gives the eigenvalues in presented in the main text.

Perturbative coupling to dark states

In the limit $\nu \to 0$, the spin profiles tend to $\tilde{\sigma}_{k_\mu}(Z) = (1/\mathcal{N}_\mu)\cos(\mu\pi Z)$ for $\mu = 0, 1, \ldots$. The coupling between the even and odd μ states are zero due to parity considerations, but the coupling of the bright state to even-μ dark states is given by

$$\frac{\mathrm{i}\sqrt{2}mn\Gamma_{\rm 1D}}{2}\int_{[0,1]^2}dZdZ'\cos(\mu\pi Z)\exp(\mathrm{i}\nu|Z - Z'|) = \frac{mn\Gamma_{\rm 1D}}{2\sqrt{2}\mu^2\pi^2}\nu. \tag{26}$$

A rudimentary rate of loss to decoherence of the bright-state is then given as the sum of these rates for $\mu = 1, \ldots$, i.e., $\frac{N\Gamma_{\rm 1D}}{12\sqrt{2}}\nu$ which yields the result of the main text upon replacement of ν and approximation $\pi/(3\sqrt{2}) \approx 1$.